In-operando X-ray scattering characterization of smectite swelling experiments

Roy Chaaya, Stephane Gaboreau, F. Milet, Nicolas Maubec, Joachim Tremosa, Hugues Raimbourg, Eric Ferrage

Applied Clay Science 245 (2023) 107124

Contents lists available at ScienceDirect

Applied Clay Science

journal homepage: www.elsevier.com/locate/clay

Research Paper

In-operando X-ray scattering characterization of smectite swelling experiments

R. Chaaya [a,b], S. Gaboreau [a,*], F. Milet [b], N. Maubec [a], J. Tremosa [a], H. Raimbourg [b], E. Ferrage [c]

[a] BRGM, F-45060 Orléans Cedex 2, France
[b] Observatoire des sciences de l'Univers (ISTO), Campus Géosciences, 1A rue de la Férollerie, 45071 Orléans, France
[c] UMR CNRS 7285 IC2MP, Université de Poitiers, Equipe HydrASA, 5 rue Albert Turpain, Bat B8, 86022 Poitiers, France

ARTICLE INFO

Keywords:
Smectite
Hydration
Swelling capacity
In-operando
X-ray scattering
Microstructure

ABSTRACT

Swelling capacity of smectite was studied over decades regarding its application as barrier in disposal of nuclear wastes in geological repositories as well as the induced volume change potential in soils according to moisture. In order to improve our knowledge in the swelling capacity of smectite, a miniaturized oedometer was developed to combine swelling pressure measurement with wide angle X-ray scattering (WAXS) characterization in real time during hydration of smectite. This coupled set up allowed studying hydration of smectite up to saturation under confined condions and linking crystalline swelling to pressure at various densities. The modeling of the WAXS patterns gave also quantitative information about the relative proportion of the different interlayer water types at saturation. In situ and operando data were acquired for homo-ionic Na^{+}- and Ca^{2+}-exchanged smectite at two different densities (1.5 and 1.8 g/cm^3). The results showed that the swelling pressure rise was correlated to a sequence of water layer type with the transition from 0W to interstratification of 2W/3W layers, depending on the density. The cation valency controlled the rate of hydration with faster hydration in the case of divalent exchanged smectite. At saturation, with increasing density, the amount of 3W layers decreased to the gain of 1W and 0W layers. Results also confirmed that at saturation and a density of 1.8 g/cm^3, the interlayer porosity represented the total one. Finally, this development provided opportunity to improve our knowledge in the swelling mechanism of compacted swelling clay materials upon hydration.

1. Introduction

Clay swelling and microstructure change are crucial parameters in the hydro-mechanical and chemical coupling behavior in compacted clayey materials used in engineered barriers in many environmental and energy applications (i.e. oil and gas recovery, building materials, environmental remediations and radioactive waste disposal).

The swelling capacity of clays is mainly due to the abundant presence of smectite, a 2:1 phyllosilicate in soils or bentonite (Bergaya and Lagaly, 2013). The structure of swelling 2:1 or TOT phyllosilicates consists of a parallel stacking of layers separated by an interlayer. The layer structure is represented as one octahedral sheet (O) sandwiched between two tetrahedral sheets (T). In the tetrahedral and octahedral sheets, the isomorphic substitution of cations by others of lower valency results in a permanent negative charged layer, compensated by cations in the interlayer. The solvation of these counterions, adsorbed on the interlayer surface clay sheets, plays a major role in the swelling properties of clays, depending on cations, density and/or the volume expansion limits.

The two main mechanisms responsible for the swelling of smectite-based materials are most often referred as crystalline and osmotic swelling (Laird, 1996, 2006; Laird et al., 1995; Liu, 2013; Luckham and Rossi, 1999; Meleshyn and Bunnenberg, 2005; Norrish, 1954) also called disjoining pressure (Gonçalvès and Trémosa, 2010). Crystalline swelling results in an increase of the interlayer as a function of the activity of water and evolves from 9.5 to 10.0 Å at the dry state (0W layer) to 12.3–12.7 Å for one layer of water molecules (1W layer), 15.0–15.8 Å for 2 layers (2W layer) and 18.0–18.9 Å for 3 layers (3W layer), depending on the interlayer cations (Dazas et al., 2014; Ferrage et al., 2005a; Laird, 2006; Likos and Wayllace, 2010; Villar, 2007). The 4W hydration state is uncommon and has only been reported for Wyoming-type bentonite, not for homo-ionic Na- or Ca-montmorillonites and only in dilute systems (Fernández and Rivas, 2005; Norrish, 1954; Saiyouri et al., 2018).

* Corresponding author.
E-mail address: s.gaboreau@brgm.fr (S. Gaboreau).

https://doi.org/10.1016/j.clay.2023.107124
Received 28 April 2023; Received in revised form 29 August 2023; Accepted 2 September 2023
Available online 8 September 2023

The swelling that occurs beyond an interlayer spacing of 40 Å in dilute solution is called osmotic swelling (Norrish, 1954; Wang et al., 2011; Wang et al., 2022; Zhang and Low, 1989). Interlayer spacing for sodium montmorillonites rapidly exceeds 40 Å and then progresses linearly with increasing water content (Meleshyn and Bunnenberg, 2005; Michot et al., 2004; Norrish, 1954). This swelling is associated with the development of osmotic repulsive forces as the system tends to reach the saturation state. More precisely, these electrostatic interactions are generated between the clay layers but also between the montmorillonite particles (Chapman, 1913; Gouy, 1916; Gouy, 1910; Lubetkin et al., 1984; Stern, 1924). Note that the internal osmotic swelling could result in the subdivision of clay particles into smaller particles consisting of only 1 to 2 layers, so called tactoids in the case of a dilute system (Bergaya and Lagaly, 2013; Lagaly, 1993; Laird, 2006; Segad et al., 2012). This is not the case for divalent smectites where the osmotic swelling is significantly restrained in the interlayers due to the high bonding energy of the divalent cations (Jellander et al., 1988; Wang et al., 2011).

In confined conditions, the swelling force generated during the hydration of smectite at constant volume is thus the contribution of repulsive forces mainly composed of both crystalline and osmotic swelling regimes. The expression of these different contribution to overall swelling process depends on the distance between adjacent particles and on various physico-chemical parameters such as density, nature of interlayer cations, ionic strength and temperature (Bag and Rabbani, 2017; Karnland et al., 2006).

Smectite hydration has been extensively characterized by X-ray diffraction (XRD) to understand the evolution of the interlayer distance under variable activity of water (Bérend et al., 1995; Ferrage et al., 2005a; Ferrage et al., 2010; Glaeser and Méring, 1954; Glaeser and Méring, 1968; Harward and Brindley, 1964; Harward and Carstea, 1967; Laird, 1996; Norrish, 1954; Sato et al., 1992; Sposito and Prost, 1982; Tamura et al., 2000; Watanabe and Sato, 1988; Yamada et al., 1994). Given the difficulty of performing XRD acquisitions during hydration in confined conditions, most of these analyses were carried out on clay powders or dispersed oriented preparations under free swelling conditions. Few studies to date have reported diffraction data on crystalline swelling of montmorillonite saturated either directly from the aqueous phase or through water vapor adsorption under confined conditions. XRD devices, in reflection configuration, have been developed to follow swelling pressure simultaneously to hydration evolution (Takahashi et al., 2015; Viani et al., 1983; Wang et al., 2011; Wang et al., 2022). Torikai et al. (1996) studied the thermodynamic properties of water in compacted sample and Ichikawa et al. (2004) the effect of consolidation on saturated bentonite at dry densities of 1.2 and 1.4 g/cm^3, respectively. Kozaki et al. (1998) and Kozaki et al. (2010) were interested in the diffusion of ions in compacted montmorillonites according to density (1.0–1.8 g/cm^3). All these studies characterized the presence of interstratification with three and two layer hydrate. Muurinen et al. (2004) used small angle X-ray scattering (SAXS) to study Wyoming bentonite microstructure and anion diffusion. Devineau et al. (2006) and Holmboe et al. (2012) studied the hydration of smectite Wyoming bentonite. Both reported the presence of three layers of water up to density of 1.7 g/cm^3. Villar et al. (2012) studied the basal spacing of two compacted bentonites with divalent cations (FEBEX bentonite) and monovalent one (MX-80). They reported different hydration behavior, according to water content and cation valency, with the interstratification of different layers of hydrates. Nevertheless, the samples were dismanteled prior to X-ray acquisitions. The study of Holmboe et al. (2012) and Warr and Berger (2007) are the sole to date to have modeled the experimental X-ray patterns and proposed a distribution of layer hydrates from various densities. Holmboe et al. (2012) reported that the transition between crystalline and osmotic interlayer swelling (i.e. basal spacings >19 Å) occured at density below 1.4 g/cm^3 for Na^+-exchanged smectite, as previously shown by Muurinen (2009). But, as for some previous studies the confinement condition was not maintained during the XRD acquisitions. Most of these published data gave key insights in the hydration mechanism of smectite according to dry densities and type of counterions, despite none of them provided quantitative description of hydration state correlated to macroscopic behavior such as the swelling pressure measurement. The objective of this research is to use laboratory-scale small angle X-ray scattering and wide angle X-ray scattering (SAXS/WAXS) set up in combination with in-situ and operando miniaturized oedometers to study in real time hydration of Na^+- and Ca^{2+}- smectites at different dry densities, to link for the first time the evolution of the crystal structure, with modeled quantitative data of hydration state, to the development of swelling pressure in confined conditions from dry to fully saturated states.

2. Materials and methods

2.1. Samples

The smectite used for this study was the Kunipia-G, a highly pure montmorillonite (>95%) (Kozaki et al., 1998; Sato, 2008; Wilson et al., 2004) provided by Kunimine Industries and issued from the purification of the natural bentonite Kunigel-V1. The structural formula of this montmorillonite $Na_{0.41}K_{0.01}Ca_{0.04}(Si_{3.92}Al_{0.08})(Al_{1.51}Mg_{0.37}Fe_{0.12})O_{10}(OH)_2,nH_2O$ with a negative layer charge of 0.5 per half unit-cell was determined by Massat et al. (2016). The same smectite batch was used in the present work.

The cation exchange capacity (CEC) is 109 cmol(+)/kg with the following distribution of exchangeable cations: Na 83%, Ca 12%, Mg 5%. The specific surface area (a_s) determined from a nitrogen adsorption experiment is 40 m^2/g, similar (45 and 42 m^2/g, respectively) to that found by Kozaki et al. (1999) and Massat et al. (2016). Based on the desorption branch of water isotherm, and assuming that interlayer is accessible, apparent total specific surface area (refered subsequently S_a) was estimated at 660 m^2/g (Massat et al., 2016), close to the value of 700 m^2/g, measured with ethylene glycol mono ethyl ether (Kozaki et al., 1999). The solid density (ρ_s) of Kunipia-G determined by helium pycnometry is 2.71 ± 0.03 g/cm^3.

The smectite was washed and homo-ionized in Na^+- and Ca^{2+} exchanged-form (saturation procedure was given in supplementary data). The CEC and cation population are given in Table 1. The exchanged samples are refered to subsequently as Na^+- and Ca^{2+}-exchanged smectites.

Both smectite samples were then oven dried for two days at 150°C and finely hand ground in an agate mortar at a grain size sieved between 25 and 32 µm.

NaCl and $CaCl_2$ solutions at a concentration of 10^{-4} mol.L^{-1} were used respectively to saturate the Na^+- and Ca^{2+}-exchanged smectite in order to avoid any possible cation exchange through the hydration process.

Table 1
Measured CECs and exchangeable cations (*ec*) for the Kunipia-G, Na^+- and Ca^{2+}-exchanged smectites.

	Cation distribution				CEC (Σ_{ec})	CEC
	Na^+(%)	Ca^{2+}(%)	Mg^{2+}(%)	K^+(%)	cmol (+)/kg	cmol (+)/kg
Kunipia-G	83	12	5	0	110	109
Na^+-exchanged smectite	95	1	4	0	108	109
Ca^{2+}-exchanged smectite	1	97	2	0	108	110

2.2. X-ray diffraction

Oriented samples, 9 mg clay/cm^2, were prepared for both Na^+- and Ca^{2+}-exchanged smectite. XRD patterns were then recorded using a Bruker D8 Advance Da Vinci diffractometer equipped with CuKα radiation ($\lambda = 1.5406$ Å) operating at 40 kV and 40 mA and a LynXeye XE 1D detector coupled to an Anton Paar CHC+ chamber and with a Modular Humidity Generator (MHG) produced by Projekt Messtechnik. Samples were measured in Bragg Brentano reflection mode over the 3.5–40°2θ CuKα angular range and a step size of 0.03°2θ. After being introduced into the CHC+ chamber, samples were maintained at the desired relative humidity (RH) over 60 min at 25°C, and were then analyzed by maintaining these (T, RH) conditions. Several acquisitions were done each 15 min to evaluate any changes of the (00*l*) Bragg positions. RH was controlled with a hygrometer located close to the sample. All acquisitions were done starting from a dry state by heating the sample at 150 °C for hours, when no deplacement of the (00 *l*) Bragg reflections are measurable. Different adsorption cycles were done step by step from dry state to 95% RH.

2.3. In-operando oedometer/WAXS coupled set up

A miniaturized oedometer set up, oedometer cell and load frame, modified from Massat et al. (2016) was developed and validated to continuously monitor the evolution of both the swelling pressure and the interlayer spacing using WAXS acquisitions throughout hydration at constant volume. The designed set up is displayed on Fig. 1.

The sample diameter was significantly reduced compared to conventional oedometers. The smectite, on which WAXS acquisitions were performed, was compacted inside a small sample holder with an inner diameter of 4.95 mm placed into the cell ring in order to obtain a reasonable acquisition time with a good signal to noise ratio. The sample height was set at 9 mm and remained constant through the hydration experiment. All the parts of the cell were machined in black polyetheretherketone (PEEK).

Swelling experiments were performed in the miniaturized oedometer cell (Fig. 1) on either Na^+- or Ca^{2+}-exchanged smectite at both dry densities of 1.5 and 1.8 g/cm^3.

Before hydration, the smectite was compacted into the cell and oven dried at 150°C for 48 h. Then, the cell was placed on a load frame to monitor the sample swelling pressure using a load sensor. Solutions were injected into the cell through the lower piston using a constant hydraulic head of 0.1 MPa. All the experiments were performed under constant volume and drained conditions and at room temperature of 25 ± 1.5°C. Vacuum was imposed inside the pistons before the beginning of each test to avoid air bubbles being trapped at the base of the sample, or in the lower piston. The dimensions and position of this swelling device were adapted to the available space in the WAXS instrument.

Several tests were carried out first in the same conditions to ensure their repeatability as well as the load sensor's sensitivity. Moreover, this device was validated by comparing our data to those acquired using a conventional standard oedometer (Fig. S1, supplementary data).

The laboratory WAXS experiments were performed at ISTO laboratory (Orléans, France) on a Xeuss 2.0 model provided by the Xenocs Company. This instrument was composed of a monochromatic molybdenum X-ray source with a wavelenght λ = 0.71078 Å and an associated $E = 17{,}8$ keV, a collimation system or scatterless enabling to focus the incident beam, a beamstop to protect detctor exposure from the direct beam intensity, a diffracted beam tube and a two-dimensional (2D) Pliatus 3R 300 K detector. For all experiments, the "high flux" collimation mode (intermediate opening of slits ((1.2 × 1.2) mm^2 and (0.8 × 0.8) mm^2) was chosen because it offers sufficient photon rate and a better counting acquisition. The sample to detector distance was 600 mm and depending on this parameter the accessible angular window ranged from 2θ = 0.18° to 10°. This range was large enough as scattered intensities for the different smectite hydrates were measured at low angles (<2°) with the considered wavelength. The beam was focalized in the middle height of the sample. Fifty scattering patterns were acquired with an exposure time of 1 h per pattern and a cycle time of 1 min between 2 successive ones.

For the data treatement, 2D images were reduced using « Foxtrot » software developed by SOLEIL synchrotron in order to previsualize, reduce and pre-analyze X-ray scattering data. The data processing method for all scattering patterns was as follows: a mask was first applied on the image to exclude all detector dead zones and dead pixels, image was second reduced using the azimuthal integration intensity function, the latter allows the conversion of the 2D Debye-Scherrer rings to a 1D diffraction pattern. Finally, only the $d_{(001)}$ Bragg reflection of

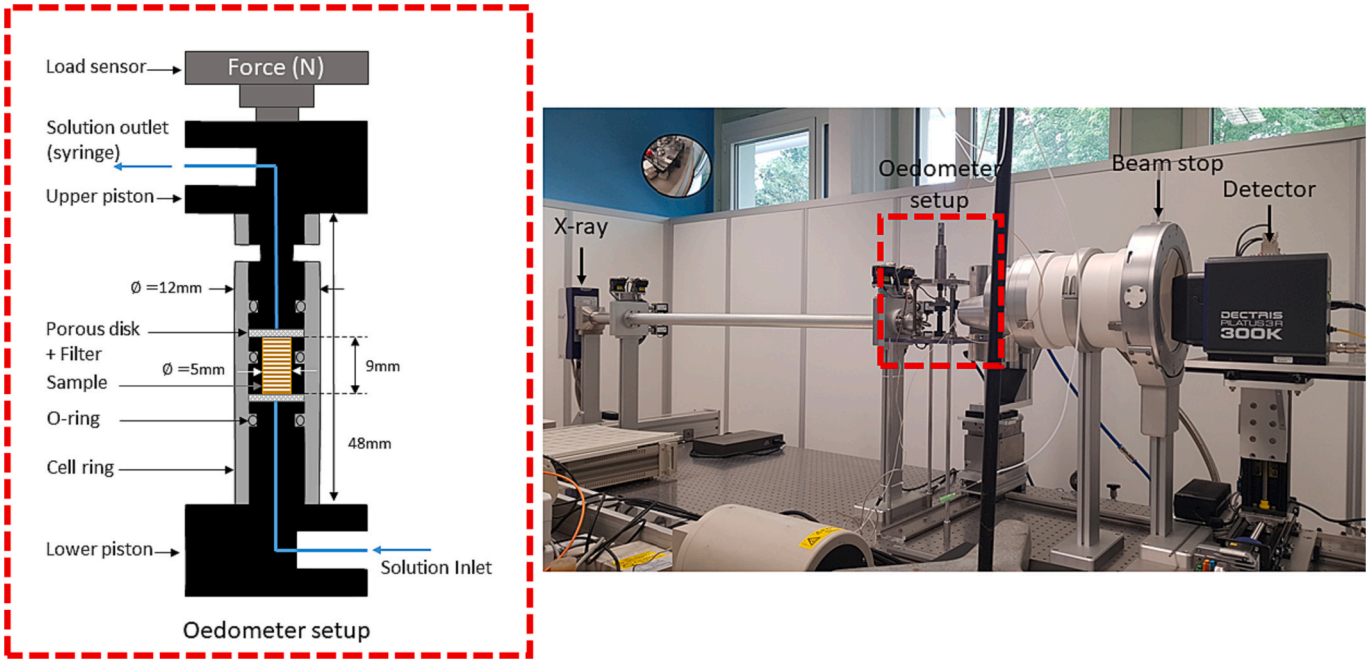

Fig. 1. Representation of the schematic layout of the oedometer cell at constant volume and (b) oedometer set up installed in the laboratory SAXS/WAXS instrument.

smectite was analyzed as the effect of platelets hydratation was specifically noticeable for this plan.

2.4. XRD patterns modeling

The experimental XRD patterns of montmorillonite were modeled in the 3–11° 2θ Cu Kα range using the algorithms developed by Sakharov et al. (1982) to determine the relative proportion of different hydration states commonly reported in smectites. In the fitting process, discrete hydration states were introduce as follows: with dehydrated layers (0W layers, layer thickness at 9.6–10.1 Å), mono-hydrated layers with one plane of H_2O molecules in the interlayer (1W layers at 12.3–12.7 Å), bihydrated layers (2W layers at 15.0–15.8 Å) and trihydrated layers (3W layers at 18.0–18.9 Å). According to the results of the fit, and to reproduce the experimental XRD pattern unique periodic structure or contribution of randomly interstratified mixed-layer structure containing different layer types can be considered. The fitting procedure was described in detail elsewhere (Ferrage et al., 2005a; Ferrage et al., 2010; Ferrage et al., 2011b). For all patterns, structural parameters, such as the number of and relative proportion of the different interstratified structures (limited to four here), their composition (relative proportions of the different layer types), and the mean number of layers in the coherent scattering domain size along the c^*-axis, were adjusted to fit the experimental XRD pattern. The mean number of layers in the coherent scattering domain sizes was found to range between 7 and 4 layers for all patterns investigated.

3. Results and discussion

3.1. XRD patterns

Fig. 2 shows the evolution of the XRD patterns as a function of RH for unconfined powders of Na^+- and Ca^{2+}-exchanged smectite. Usual discrete hydration states 00 *l* positions for smectite are superimposed on

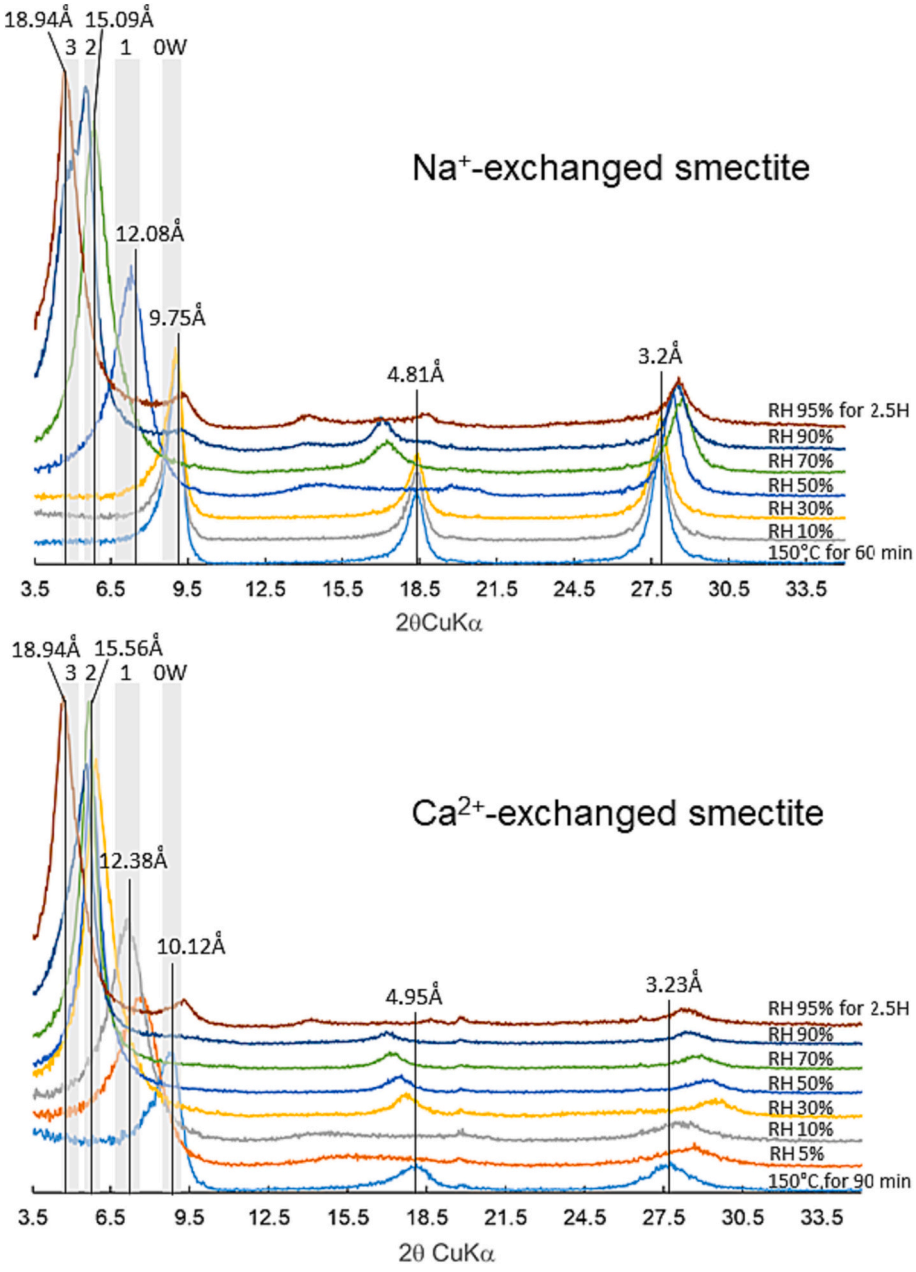

Fig. 2. Experimental XRD patterns as a function of relative humidity of Na^+-and Ca^{2+}-exchanged smectite at T=25°C. Lines indicate the position of the maxima.

Fig. 2, i.e. 0, 1, 2 and 3W layers (Ferrage et al., 2010). For both experiments (Na^+- and Ca^{2+}-exchanged smectite), the 001 reflection varied as a function of RH, with a usual stepwise evolution, starting from an hydration state close to 0W domain, with maximum intensity values at 9.75 Å, as typically observed for Na^+-exchanged smectites (Bérend et al., 1995; Cases et al., 1992; Ferrage et al., 2005b; Mooney et al., 1952; Norrish, 1954) and 10.12 Å for the Ca^{2+}-exchanged smectite. At RH of 95% both XRD patterns showed an assymetric reflection with maximum intensity values of the 001 reflection at ~18.9 Å, close to 3W layers domain. The main difference occured in the rate of hydration between Na^+ and Ca^{2+} experiments. In the case of Na^+-exchanged smectite, the transition between 0 and 1 layer of H_2O molecules occured at RH of 50%, while for Ca^{2+} experiment, the transition 0–1 layer was achieved at a RH of 10% and the two 2 layers of H_2O molecules was reached at a RH of 50%. In between these two discrete positions, different hydration states or transition between two discrete hydrations states followed one another. The broadening of the full width at half maximum intensity (FWHM), for the different XRD patterns, revealed the hydration heterogeneity (Ferrage et al., 2005b) with the coexistence of smectite layers at given hydration steps.

To determine quantitatively the relative proportions of the different layer types, the experimental XRD patterns at RH of 95% were modeled. Results are given in Table 2.

At RH of 95%, as described above with the assymetric 001 reflection, both the Na^+- and Ca^{2+}-exchanged smectites were constituted of mixed layer with quite similar proportion of 3W (63%) and 2W (28%) layers producing high angle asymmetry. Some proportions of 1W and 0W layers were still quantified. As demonstrated by Dazas et al. (2014), homogeneous 3W hydration state could be reached at RH of 98% up to 5 h ramps of hydration. It means that in conditions, imposed in this work at constant relative humidity, the samples were not fully hydrated. This difference can be tentitatively assigned to (i) the difference in RH values considered (98% in the study of Dazas et al. (2014) versus 95% RH here), and/or (ii) the lower charge of the Wyoming montmorillonite used by Dazas et al. (2014) compared to the higher layer charge of the Kunipia montmorillonite used here, which somehow limits the hydration properties of the sample (Emmerich et al., 2018).

3.2. *In situ and operando swelling experiments*

The swelling force was systematically recorded from dry to saturation states. At the same time, a cyclical WAXS acquisition was achieved to follow the hydratation of smectite. A first acquisition was carried out prior to hydration to get a reference dry state pattern. This was referred as the “Initial state”. When the measured swelling pressure reached its steady state and the scattering signal stopped evolving, the sample was considered saturated and the test stopped. Fig. 3 displays X-ray scattering patterns evolution as a function of time and so hydration of a compacted smectite sample during swelling pressure measurements.

The one dimensional scattering intensities versus q ($Å^{-1}$) (i.e. $I(q)$) presented in Figs. 4 and 5 resulted from the radial integration of the 2D data presented in Fig. 3. All the experiments were acquired with the same procedure. As described in the experimental set up, the X-ray beam was focalized on the middle height of the sample, with a beam size of 1 × 1 mm^2. The evolution of the WAXS pattern according to time gave an overview of the smectite hydration at a single point but did not allow to spatialize the water migration and did not allow to follow the hydration over the height of the sample.

Table 2
Distribution of the layers type in Na^+- and Ca^{2+}-exchanged smectite at RH ~ 95%.

	% (0w)	% (1w)	% (2w)	% (3w)
Na^+-exchanged smectite	2	7	28	63
Ca^{2+}-exchanged smectite	2	6	28	64

Results of a combined acquisition of WAXS patterns acquired simultaneously with the swelling pressure are displayed in Fig. 4.

Some selected WAXS patterns are presented on the Fig. 4a and c acquired at different time of hydration of the swelling experiment in oedometric conditions. The time of acquisitions of the different WAXS data are reported on the swelling pressure plot obtained simultaneously (Fig. 4b and d). At initial state, the smectite was characterized by a strong Bragg reflection position at $q = 0.65$ $Å^{-1}$ (Fig. 4a and c) in the WAXS region, corresponding to the (001) d-spacing ($d_{(001)}$) of 9.6 Å. With increasing time, and so hydration of the smectite, WAXS patterns shifted toward smaller q values, indicating higher d-spacings. After 4 h of hydration, the diffraction pattern displayed a broadening with hump at low angle compared to the initial state. Over time, the position of the d-spacing shifted progressively at $q \approx 0.51$, 0.4 and 0.35 $Å^{-1}$, corresponding to apparent d-spacing with maximum intensity values at 12.3, 15.7 and 17.9 Å. Beyond 20 h, the WAXS signal did not present any evolution with a large diffraction peak ranging from 0.52 up to 0.32 $Å^{-1}$, i.e., 12.06 to 19.5 Å.

At the same time, the swelling pressure of Na^+-exchanged smectite compacted at a density of 1.5 g/cm^3 rapidly increased once the hydration process started and then reached a quasi constant value (5 MPa) within approximately 3 h. The swelling pressure raised again around 10 h until reaching a steady state regime at a pressure of 6.5 MPa over 18 h. This stepwise swelling pressure curve, with two distinct steps, was typical to those described in the literature (Gens et al., 2011; Imbert and Villar, 2006; Komine and Ogata, 2003; Massat et al., 2016; Pusch, 1982; Schanz and Tripathy, 2009; Wang et al., 2022).

The same protocol was applied at a dry density of 1.8 g/cm^3. The WAXS and swelling pressure results were overlayed on the data obtained at a density of 1.5 g/cm^3 (Fig. 4). The WAXS patterns displayed the same behavior with a progressive shift toward smaller q values upon hydration. Over time, the position of the d-spacing shifted at $q \approx 0.4$ and 0.35 $Å^{-1}$ progressively, corresponding to d-spacing of 15.7 and 17.9 Å. No transition at $q \approx 0.51$ $Å^{-1}$ were measured for this density. The associated swelling pressure experiment displayed a similar aspect than the test done at 1.5 g/cm^3, with a double step evolution. This latter was not so marked in the case of Na^+-exchanged smectite compacted at a density of 1.8 g/cm^3. More particularly, the corresponding swelling pressure rised very quickly in the first hour, but then proceeded to increase more slowly until it reached the equilibrium value (i.e. 14.34 MPa) up to 44 h. The occurrence or not of this double step aspect was identical to that found by Cho et al. (2000).

Experiments were also perfomed with the Ca^{2+}-exchanged smectite at both 1.5 and 1.8 g/cm^3. The WAXS patterns acquired at $t = 0$; 3; 6; 10, 20 and 44 h while monitoring the swelling pressure are displayed onFigure 4. As for the Na^+-exchanged smectite, WAXS patterns followed the same evolution upon hydration with a progressive shift toward smaller q value. At initial state, the maximum intensity value of the reflection was close to 9.6 Å. After 3 h of hydration, a broadening of the diffraction signal was observed, ranging from 0.65 to 0.34 $Å^{-1}$, with no distinctive discrete position. According to time increase, the (001) d-spacing shifted progressively at $q \approx 0.51$, 0.4 and 0.34 $Å^{-1}$, corresponding to d-spacing of 12.3, 15.7 and 18.5 Å. Concurrently, swelling pressure was monitored following the same behavior as Na^+-exchanged smectite, except that Ca^{2+}-exchanged smectite generated higher pressures. As in the case of Na^+-exchanged smectite at a density of 1.8 g/cm^3, no stepwise evolution was observed for both swelling experiment of Ca^{2+}-exchanged smectite at densities of 1.5 and 1.8 g/cm^3. At 1.5 g/cm^3, the swelling pressure increased rapidly once the hydration process started then reached a short steady state at 7 MPa within almost three hours. The swelling pressure started to increase again up to 6 h and stabilized at 8 MPa over 10 h (Fig. 4). For Ca^{2+}-exchanged smectite compacted at a density of 1.8 g/cm^3; the swelling pressure increased in a quasi-monotonic way to stabilize at around 16.2 MPa within approximatively 20 h.

The different swelling pressures probed for the four set of data were

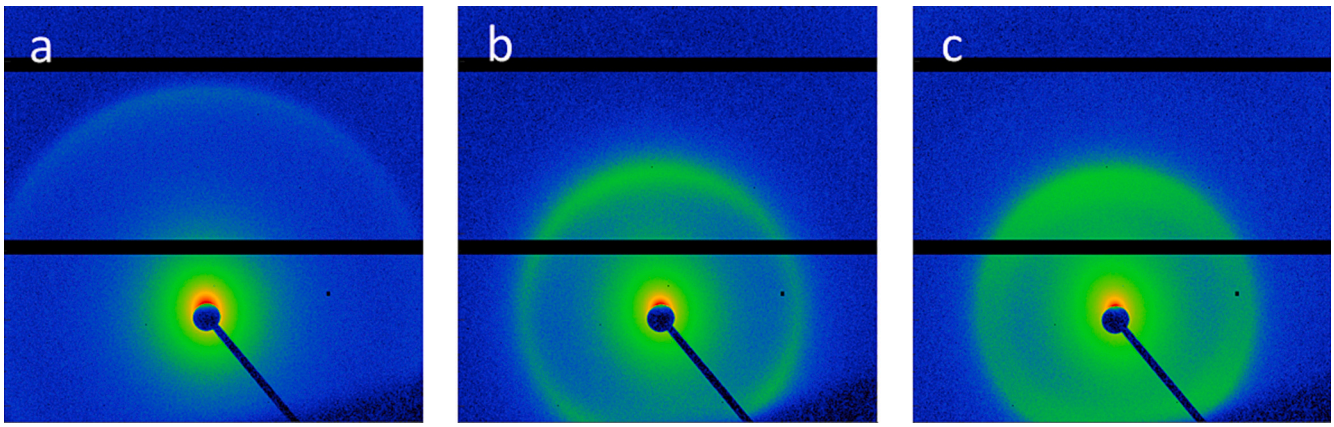

Fig. 3. 2D WAXS patterns for the compacted smectite at initial dry state (a), after 10 (b) and 20 h of hydration (c).

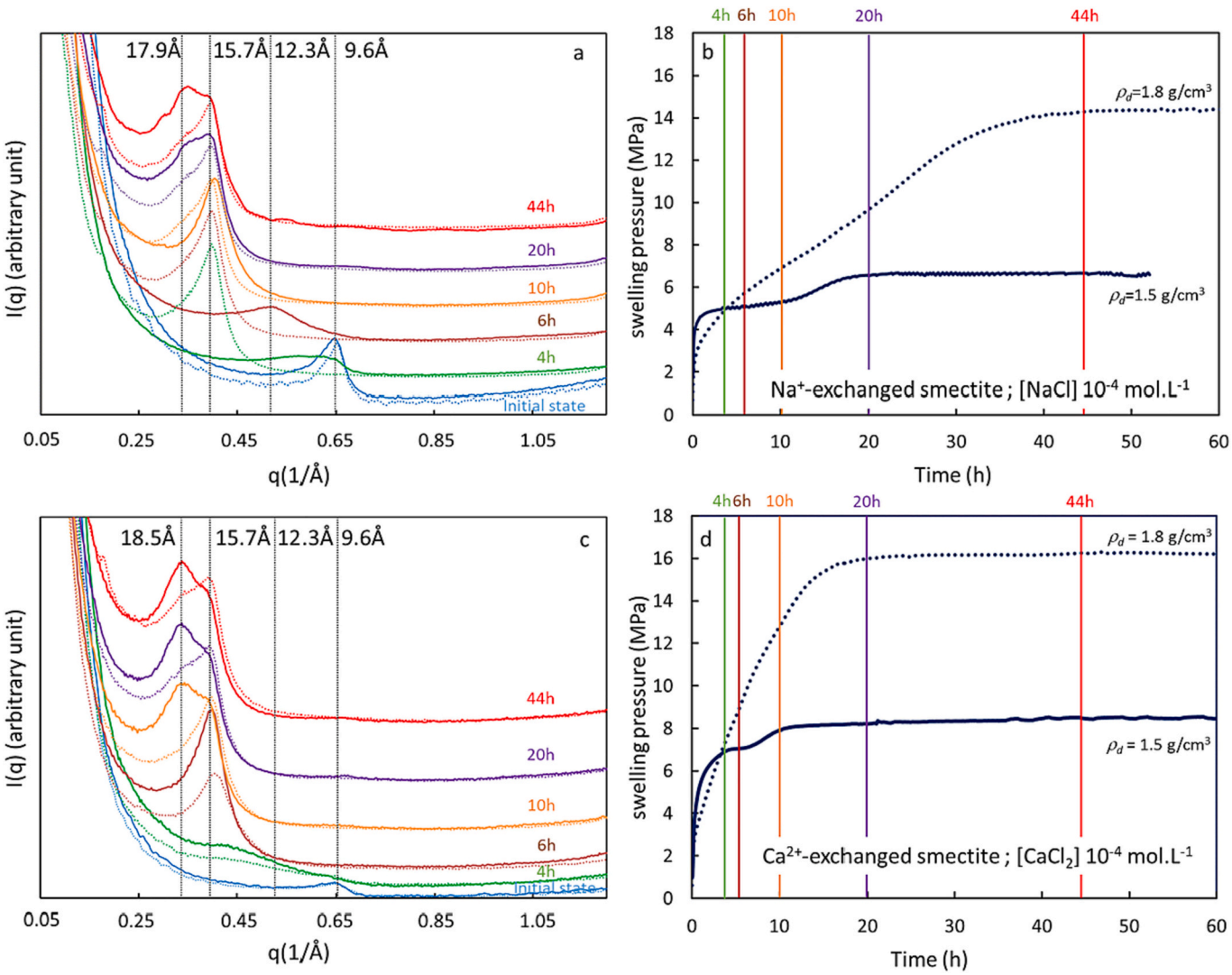

Fig. 4. In-operando WAXS acquisitions and swelling pressure experiment during hydration of Na^+ and Ca^{2+}-exchanged smectite with a solution of NaCl and $CaCl_2$ at a concentration of 10^{-4} mol.L^{-1} compacted at a dry density of 1.5 (solid line) and 1.8 (dotted line) g/cm^3. (a) 1D WAXS patterns and (b) swelling pressure of Na^+-exchanged smectite; (c) 1D WAXS patterns and (d) swelling pressure of Ca^{2+}-exchanged smectite.

in good agreement with the published data and the exponential behavior according to increasing dry density (Karnland et al., 2006; Massat et al., 2016; Schanz and Tripathy, 2009; Villar et al., 2012). Regardless the density, the swelling pressure of Ca^{2+}-exchanged smectite was always higher than Na^+ one.

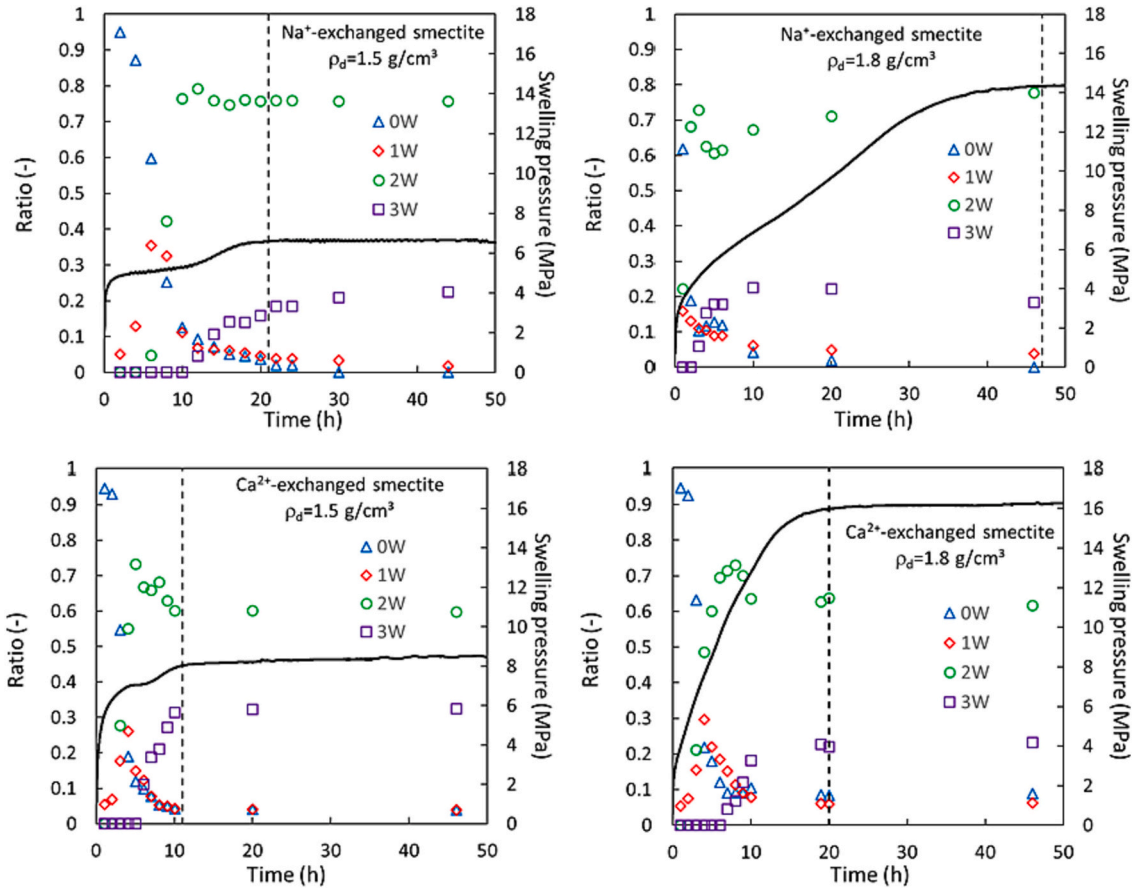

Fig. 5. Distribution of water interlayer types for the four set of swelling pressure experiments as a function of time.

3.3. WAXS patterns modeling results

Fig. 5 shows the relative proportion of the different interlayer types obtained for the four sets of swelling experiments (Na^+-exchanged smectite at 1.5 and 1.8 g/cm^3 and Ca^{2+}-exchnaged smectite at 1.5 and 1.8 g/cm^3) over time. An example of comparisons between experimental and calculated profiles on selected XRD patterns is reported in supplementary data (Fig. S2). The methodology, extensively validated on a large number of samples and experimental conditions (Dazas et al., 2014; Dazas et al., 2015; Ferrage, 2016; Ferrage et al., 2005a; Ferrage et al., 2005b; Ferrage et al., 2011a; Kelch et al., 2019; Kelch et al., 2021) was found to be sufficient to reproduce all patterns collected in the present study (Fig. 5). The three experiments started in dry conditions with 95% of 0W states. In the case of Na^+-exchanged smectite at a density of 1.8 g/cm^3, the initial state consisted of 62% of 0W layer, 16% of 1W layer and 22% of 2W layer, indicating that the sample was partially hydrated at the starting of the experiment.

Starting from the lowest dry density investigated, 1.5 g/cm^3, for the Na^+-exchanged smectite, the first swelling pressure increase was concomitant to the development of 1W state up to 35% of layers. At this maximum of 1W state, a gradual increase of 2W layers proceeded, while the 1W layers decreased, and reached 80% of layers to stabilize at a value close to 75%. The stabilization of the 2W state corresponded to the increase of the 3W state and coincinded to the second swelling pressure increase. Over 20 h of experience, the swelling pressure stabilized and the modeling of the WAXS patterns gave similar ratio with a hydration state composed of 75% of 2W layers and 22% of 3W layers. A small amount of 1W layers was always quantified.

In the case of Ca^{2+}-exchanged smectite, at the same density, quite the same sequence of hydration was observed. The first increase of the swelling pressure was concomitant to the increase of 1W state. In this experiment, the increase of the 2W layers started at almost the same time than the 1W state. The proportion of 1W layers decreased while the 2W layers gradually increased up to a maximum of 73%. At this time of experiment, the 3W layers gradually increased as well as the second swelling pressure increased, associated to a decrease of the 2W layers before stabilizing at 60%. As for the previous experiment, the swelling pressure stabilized and the modeling of the WAXS patterns gave similar ratio with a hydration state composed of 60% of 2W layers and 32% of 3W layers. As for the previous test on Na^+-exchanged smectite, small amounts of 1W and 0W layers were detected (~4%).

At the highest dry density, for both Na and Ca experiments, the stepwise evolution of the swelling pressure was not so marked. The swelling pressure increased gradually before reaching a steady state behavior. This evolution was consistent with a rapid increase of the 1W state, concomitant with the 2W state. Like for the lowest densities, two distinct steps of hydration were evidenced, i.e., the decrease of the 1W layers with the increase of the 2W layers and the stabilization of the 2W state with the increase of 3W layers.

In the case of Na^+-exchanged smectite, the swelling pressure tended to stabilize over quite 50 h with a hydration state of the smectite particles mixed of 78% of 2W, 18% of 1W and 4% of 0W layers. For the Ca^{2+}-exchanged smectite, the swelling pressure reached a maximum over 20 h with a ratio of water layers consisting of ~61% of 2W, ~23% of 3W, 9% of 0W and 6% of 1W layers. All these results were consistent with previous published data (Holmboe et al., 2012; Villar et al., 2012) showing the interstratification of 2W and 3W layers at similar dry densities. The stabilization period, i.e., period over which the swelling pressure reached a maximum, was divided by 2 in the case of Ca^{2+}-exchanged smectite experiments, in comparison with Na^+-exchanged smectite results. This behavior was already described by (Villar et al. (2012) with a faster transition from the 1W to 2W layers in the case of

divalent bentonite. At the same time, the stabilization period was twice for the highest densities compared to experiments done at density of 1.5 g/cm^3.

The relative proportion of different interlayer water types is summarized in Table 3. The data are given for the four set of experiments, when the swelling pressure was stabilized, i.e. in water saturated conditions of the samples. The overall crystalline swelling is also given in Table 3. The latter consisted of the overall mean interlayer distance calculated as the mean *d*-spacing (9.6, 12.5, 15.5 and 18.9 Å) of different layer types (0W, 1W, 2W, 3W) weighted by their respective relative proportion. In both Na^+ experiments, the relative proportion of 2W layers was quite similar with a value close to 76%. The difference was the decrease of 3W layers with the increase of the density concomitant to the increase of 1W state. This led to a small decrease of the overall crystalline swelling. In the case of Ca^{2+} experiments, the same behavior was observed with the same proportion of 2W layers close to 60% for both densities and the decrease of 3W layers with the higher density leading to the slight increase of 1W and 0W layers (Table 3). These relative proportions were totally different from what was obtained in the case of non-confined acquisition with the predominance of 3W layers (Fig. 2, Table 2).

The distribution of water interlayer types was coherent with published data (Holmboe et al., 2012; Villar et al., 2012) with the interstratification of different layers of hydrates in the range of the studied densities. The ratio between 2W and 3W of layers was somewhat different from values published by Holmboe et al. (2012), for which 3W states were predominant.

3.4. Microstructural model

In the literature, different microstructural models have been proposed (Holmboe et al., 2012; Liu, 2013; Madsen, 1998; Pusch et al., 1990; Sauzeat et al., 2001) to estimate the contribution of the different porosity domains that constitute compacted bentonite (interlayer, interparticle porosities…). Considering layer stacking geometric approach or mass balance, models could be formulated based on some hypothesis or approximation due to the lack of quantitative data. Studying saturated compacted swelling materials was challenging and some microstructural properties, as the interlayer distance at saturation, without loosing the confinement, were not well established.

Madsen (1998), based on the layer stacking theory of Pusch et al. (1990), reported values of interlayer water contribution as a function of dry density and showed that above 1.6 g/cm^3 the total porosity corresponded to the interlayer water content. Based on the latter geometric assumption, considering a homogeneous system with the same distribution of layers in stacks and in the case where the interlayer porosity equaled the total ones, Sauzeat et al. (2001) proposed the following equation (Eq. 1) estimating the maximum theoretical interlayer distance ($d_{max}(001)$) as:

$$d_{max}(001) = \frac{d_{(001)_d}}{\left(\frac{1}{\varnothing_T} - 1\right)} + d_{(001)_d} \quad (1)$$

with the total porosity:

$$\varnothing_T = 1 - \frac{\rho_d}{\rho_s} \quad (2)$$

where $d_{(001)_d}$ is the dry interlayer distance (9.6 Å), ρ_d is the dry density and ρ_s the solid density. In the case of swelling clay minerals, while constant ρ_s were used in the determination of physical properties (degree of saturation, soil water density) in soil sciences; different solid densities could be considered. In dry state, interlayer could be considered as part of the volume of a stack of layers. From this assumption, theoretical solid density, calculated as the ratio between the mass and the volume of a layer, is close to 2.7 g/cm^3, considering a thickness of two successive layers of ~9.6 Å. This value is in agreement with the one obtained with He pycnometry (2.71 ± 0.03 g/cm^3). In hydrated condition, interlayer space become accessible to water and can be considered as part of external volume. In this case, the TOT layer can be defined as the distance between two planes of apical oxygen atoms (6.54 Å, Moore and Reynolds., 1989), plus the ionic radii of two oxygen atoms (1.38 Å, Shannon and Prewitt, 1969). One should keep in mind, however, that this theoretical dimension (9.3 Å) represents an overestimated value that does not account for the irregular surface of clay minerals. Water molecules can indeed insert closer to the surfaces (i) in between two oxygen aoms or (ii) to a larger extent inside the ditrigonal cavities of the basal surfaces (Sposito et al., 1999). Accordingly, a volume fraction of the 9.3 Å TOT layer theoretical dimension remains accessible to water molecules in hydrated conditions. By stipulating that ~25% of the oxygen radii are impacted by water molecules insertion, the TOT layer theoretical dimension decreases to 8.6 Å, leading to an upper limit for estimated solid density of ~3 g/cm^3.

Based on these two previous theoretical values, the estimation of the maximum theoretical interlayer distance was done with both values (2.7 and 3 g/cm^3) and is displayed in Fig. 6a.

The same estimation of (d_{max}(001) was done from the equation given by Holmboe et al. (2012) considering uniform discrete planar surfaces and total specific surface area (S_a):

$$d_{max}(001) = \frac{1}{\left(\rho_d \times \frac{S_a}{2}\right)} - d_{(001)_d} \quad (3)$$

For the montmorillonite used in this study, *Sa* was considered at apparent values of 660 and 700 m^2/g, obtained on Kunipia-G sample (Massat et al., 2016; Kozaki et al., 1999). Fig. 6 displays the d_{max}(001) calculated from Eq. 1 and 3 and the crystalline swelling (Table 3) obtained in this study. Both formalisms are in quite good agreement when considering values of ρ_s higher than 2.7 g.cm^{-3}. This could be explained by the fact that the latter reflects dry state, while values of d_{max}(001) calculated from eq. 3 are obtained from fully accessible planar surfaces (saturated conditions). Average basal spacing obtained from the present data are plotted in Fig. 6. At a density of 1.8 g/cm^3, the average basal spacing was consistent with theoretical estimation when considering a valueof ρ_s of 3 g/cm^3, in agreement with the theoretical one at saturation (3 g/cm^{-3}) and a value of S_a at 660 m^2/g.); while when considering a ρ_s of 2.7 g/cm^3 the measured average basal spacing is higher than the value calculated from eq. 1. It means that at a density of 1.8 g/cm^3, the total porosity is closed to the interlayer volume. At a density of 1.5 g/cm^3, the calculated average basal spacing of 16.1 Å implied that interlayer volume represents 80% of the total porosity.

Table 3
Distribution of water interlayer types for the four set of swelling pressure experiments at saturation and associated calculated crystalline swelling (average basal spacing).

	Dry density (g/cm^3)	% 0W	% 1W	% 2W	% 3W	Crystalline swelling (Å)*
Na^+-exchanged	1.5	0	1.8	75.8	22.4	16.1
Na^+-exchanged	1.8	0	3.9	77.8	18.3	15.9
Ca^{2+}-exchanged	1.5	3.9	3.9	59.7	32.5	16.1
Ca^{2+}-exchanged	1.8	8.8	6.2	61.6	23.2	15.4

* crystalline swelling was calculated considering theoretical 0W, 1W, 2W and 3W states at values of 9.6, 12.5, 15.5 and 18.9 Å.

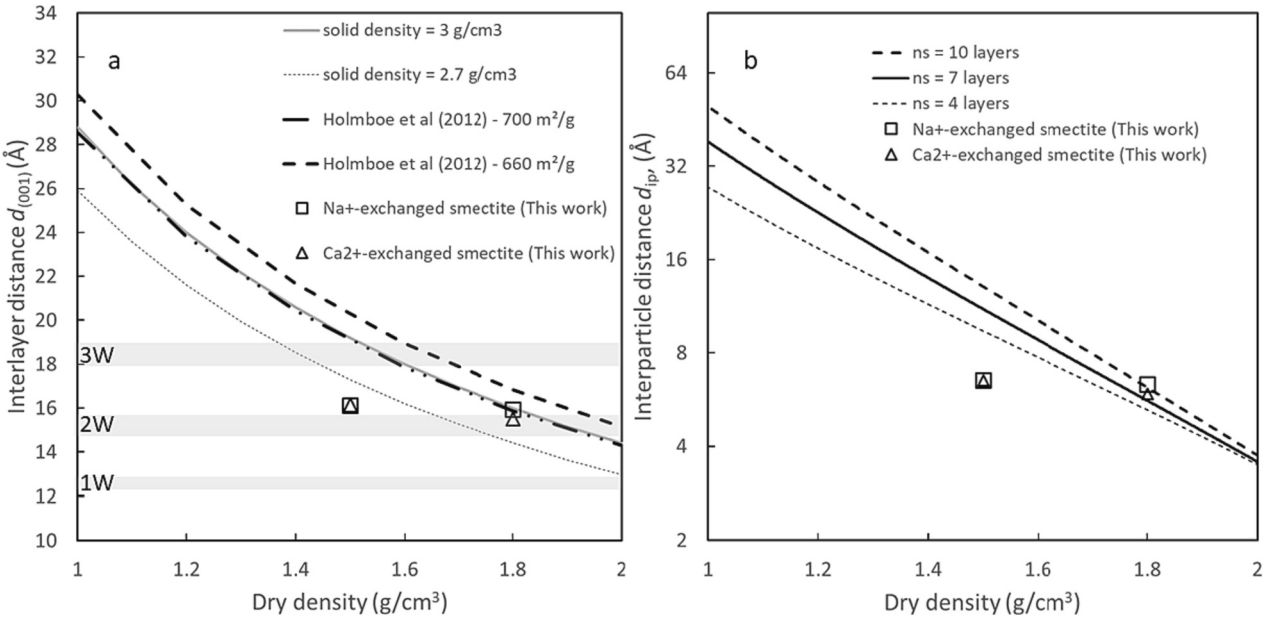

Fig. 6. A-Theoretical interlayer distance considering that total porosity was occupied by the interlayer according to the dry density. The theoretical interlayer distance for 1W, 2W and 3W states is added as indication. B-Theoretical interparticle distance according to the dry density.

In a similar way, based on the same geometric assumptions of discrete layer stacking, Liu (2013) proposed a model, which enabled, among other properties, estimating the distance between montmorillonite particles. The formalism took care of the void ratio and number of layers (n_s) constituting a montmorillonite stack. The expression considered an average and homogeneous interlayer distance. Interparticle distance (d_{ip}) was calculated according to dry densities (variable void ratio) for different n_s and with an average interlayer distance of 16 Å, coherent with the results of the present work (Table 3). The results are shown in Fig. 6. Interlayer distances, acquired from the four sets of experiment at saturation, are reported in Fig. 6. This comparison between estimated interparticle and measured average interlayer distances allowed confirming that at a density of 1.8 g/cm^3, the interparticle distance equaled the interlayer one, meaning that all the porosity was occupied by the interlayer.

This new result highlights the assumption that ρ_s of swelling clay minerals is different from dry to saturated states. This consideration could impact the estimation of some basic physical properties of soils like degree of saturation, water content or water density. Zhang and Lu (2018) proposed a critical review on soil water density to explain discrepancies existing in soil water density (ρ_w). Nonetheless most of the discussed ρ_w data (Zhang and Lu., 2018) were obtained considering dry state ρ_s values, as the degree of saturation larger than 100% in bentonite (Villar and Lloret, 2004) corrected by a density of ρ_w *higher than* 1. In soil science degree of saturation is estimated according to water density and dry state solid density (eq. 4) and most of the time ρ_w was the lonely adjusted parameter to reach 100% of saturation, while the increase of ρ_s with clay swelling could also be an additional parameter in the explanation of degree of saturation larger than 100% in the case of swelling clay materials (Villar and Lloret, 2004).

$$S_r = \frac{W}{\left(\frac{1}{\rho_d} - \frac{1}{\rho_s}\right) \times \rho_w} \quad (4)$$

4. Conclusion

A miniaturized oedometer set up was developed in the present work to acquire in operando and in real time coupled data of swelling pressure and wide angle X-ray scattering (WAXS) pattern to follow the hydration of smectites, without any volume deformation. Na^+- and Ca^{2+}-exchanged smectite, compacted at dry densities of 1.5 and 1.8 g/cm^3, were used to give insights into the dynamic evolution of the compacted montmorillonite-water system from a dry to a saturated state. All the WAXS data were modeled and provided quantitative data in the proportion of interlayer water types over time and at saturation.

The combined acquisitions of laboratory-scale WAXS patterns and swelling pressure allowed thus deciphering a sequence of hydration correlated to the stepwise evolution of the smectite swelling pressure at low density (i.e. 1.5 g/cm^3). The sharp rise of swelling pressure was concomitant with the development of 1W layer, up to the formation of 2W layers. At this step, the development of 3W layers was correlated to the second increase of swelling pressure, up to the steady state. Hydration of divalent cation led to faster transition from the 1 to the 2W layers and thus to the rise of swelling pressure and also to higher swelling capacity. The latter could be related to the higher ratio of 3W layers. At saturation, the interstratification of 2W and 3W layers was modeled for the four set of experiments with more or less 1W and 0W layers. The water type's ratio depended on the densities, with a decrease of 3W layers with increasing density, correlated to the increase of 1 and 0W layers.

These sets of data contributed to improve our knowledge in the microstructure of compacted and water saturated smectite, which is a proxy of bentonite. From the overall crystalline swelling calculated from the acquired data (Table *3*), the density of the smectite particle could be estimated to be close to 3 g/cm^3 at saturation. At a density of 1.8 g/cm^3, the overall crystalline swelling of 16 Å confirmed that the total porosity was controlled by the interlayer with an interlayer thickness of 0.64 nm.

Over these results, the successful development of this miniaturized oedometer coupled to laboratory-scale WAXS acquisitions and the quantitative distribution of water interlayer type gave access to high quality in situ diffraction data of hydrated swelling clay materials under confined conditions. In situ and operando oedometer experiments will allow to acquire hydration data in real time and provide key insight in the crystalline/osmotic mechanism of engineered barriers.

CRediT authorship contribution statement

R. Chaaya: Data curation, Writing – original draft. **S. Gaboreau:** Supervision, Writing – review & editing. **F. Milet:** Data curation. **N.**

Maubec: Data curation. **J. Tremosa:** Supervision. **H. Raimbourg:** Supervision, Resources. **E. Ferrage:** Software, Writing – review & editing.

Declaration of Competing Interest

The authors declare that they have no known competing financial interests or personal relationships that could have appeared to influence the work reported in this paper.

Data availability

No data was used for the research described in the article.

Acknowledgement

This research was performed in the framework of the EURAD project – WP7 HITEC (http://www.ejp-eurad.eu/), which receives funding from the European Union's Horizon 2020 research and innovation programme under grant agreement No 847593. The authors gratefully acknowledge Rémi Champallier for providing experimental support for the combined WAXS/swelling measurement at the ISTO laboratory. The authors acknowledge support from both LabEx VOLTAIRE (ANR-10-LABX-100-01) and EquipEx PLANEX (ANR-11-EQPX-0036) projects.

Appendix A. Supplementary data

Supplementary data to this article can be found online at https://doi.org/10.1016/j.clay.2023.107124.

References

Bag, R., Rabbani, A., 2017. Effect of temperature on swelling pressure and compressibility characteristics of soil. Appl. Clay Sci. 136, 1–7.
Bérend, I., Cases, J.-M., François, M., Uriot, J.-P., Michot, L., Masion, A., Thomas, F., 1995. Mechanism of Adsorption and Desorption of Water Vapor by Homoionic Montmorillonites: 2. The Li+ Na+, K+, Rb+ and Cs+−Exchanged Forms. Clay Clay Miner. 43, 324–336.
Bergaya, F., Lagaly, G., 2013. Handbook of Clay Science, Second Edition Ed.
Cases, J.M., Berend, I., Besson, G., Francois, M., Uriot, J.P., Thomas, F., Poirier, J.E., 1992. Mechanism of adsorption and desorption of water vapor by homoionic montmorillonite. 1. The sodium-exchanged form. Langmuir 8, 2730–2739.
Chapman, D.L., 1913. LI. A contribution to the theory of electrocapillarity. London, Edinburgh, Dublin Philos. Mag. J. Sci. 25, 475–481.
Cho, W.-J., Lee, J.-O., Kang, C.-H., 2000. Influence of temperature elevation on the sealing performance of a potential buffer material for a high-level radioactive waste repository. Ann. Nucl. Energy 27, 1271–1284.
Dazas, B., Ferrage, E., Delville, A., Lanson, B., 2014. Interlayer structure model of trihydrated low-charge smectite by X-ray diffraction and Monte Carlo modeling in the Grand Canonical ensemble. Am. Mineral. 99, 1724–1735.
Dazas, B., Lanson, B., Delville, A., Robert, J.-L., Komarneni, S., Michot, L.J., Ferrage, E., 2015. Influence of tetrahedral layer charge on the organization of interlayer water and ions in synthetic na-saturated smectites. J. Phys. Chem. C 119, 4158–4172.
Devineau, K., Bihannic, I., Michot, L., Villieras, F., Masrouri, F., Cuisinier, O., Fragneto, G., Michau, N., 2006. In situ neutron diffraction analysis of the influence of geometric confinement on crystalline swelling of montmorillonite. Appl. Clay Sci. 31, 76–84.
Emmerich, K., Giraudo, N., Schuhmann, R., Schnetzer, F., Kaden, H., Thissen, P., 2018. On the Prediction of Water Contents in Na-Saturated Dioctahedral Smectites. J. Phys. Chem. C 122, 7484–7493.
Fernández, A.M., Rivas, P., 2005. Analysis and distribution of waters in the compacted FEBEX bentonite: Pore water chemistry and adsorbed water properties. In: Alonso, L. E. (Ed.), Advances in Understanding Engineered Clay Barriers. Taylor and Francis Group, Barcelona, pp. 257–275.
Ferrage, E., 2016. Investigation of the interlayer organization of water and ions in smectite from the combined use of diffraction experiments and molecular simulations. A review of methodology, applications, and perspectives. Clay Clay Miner. 64, 348–373.
Ferrage, E., Lanson, B., Malikova, N., Plancon, A., Sakharov, B.A., Drits, V.A., 2005a. New insights on the distribution of interlayer water in bi-hydrated smectite from X-ray diffraction profile modeling of 00l reflections. Chem. Mater. 17, 3499–3512.
Ferrage, E., Lanson, B., Sakharov, B.A., Drits, V.A., 2005b. Investigation of smectite hydration properties by modeling experimental X-ray diffraction patterns: part I. Montmorillonite hydration properties. Am. Mineral. 90, 1358–1374.
Ferrage, E., Lanson, B., Michot, L.J., Robert, J.L., 2010. Hydration properties and interlayer organization of water and ions in synthetic na-smectite with tetrahedral layer charge. Part 1. Results from X-ray diffraction profile modeling. J. Phys. Chem. C 114, 4515–4526.
Ferrage, E., Sakharov, B.A., Michot, L.J., Delville, A., Bauer, A., Lanson, B., Grangeon, S., Frapper, G., Jimenez-Ruiz, M., Cuello, G.J., 2011a. Hydration properties and interlayer organization of water and ions in synthetic na-smectite with tetrahedral layer charge. Part 2. Toward a precise coupling between molecular simulations and diffraction data. J. Phys. Chem. C 115, 1867–1881.
Ferrage, E., Sakharov, B.A., Michot, L.J., Delville, A., Bauer, A., Lanson, B., Grangeon, S., Frapper, G., Jiménez-Ruiz, M., Cuello, G.J., 2011b. Hydration properties and interlayer organization of water and ions in synthetic Na-smectite with tetrahedral layer charge. Part 2. Toward a precise coupling between molecular simulations and diffraction data. J. Phys. Chem. C 115, 1867–1881.
Gens, A., Vallejan, B., Sánchez, M., Imbert, C., Villar, M.V., Geet, M.V., 2011. Hydromechanical behaviour of a heterogeneous compacted soil: experimental observations and modelling. Geotechnique 61, 367–386.
Glaeser, R., Méring, J., 1954. Sur le rôle de la valence des cations échangeables dans la montmorillonite. Bull. Mineral. 519–530.
Glaeser, R., Méring, J., 1968. Domaines d'hydratation des smectites. Comp. Rendus de l'Acad. des Sci. Paris 267, 463–466.
Gonçalvès, J., Trémosa, J., 2010. Estimating thermo-osmotic coefficients in clay-rocks: I. Theoretical insights. J. Colloid Interface Sci. 342, 166–174.
Gouy, M., 1910. Sur la constitution de la charge électrique à la surface d'un électrolyte. J. Phys. Theor. Appl. 9, 457–468.
Gouy, G., 1916. Sur la fonction électrocapillaire. Ann. Phys. 9, 5–36.
Harward, M.E., Brindley, G.W., 1964. Swelling properties of synthetic smectites in relation to lattice substitutions. Clay Clay Miner. 13, 209–222.
Harward, M.E., Carstea, D.D., 1967. Properties of vermiculites and smectites: expansion and collapse. Clay Clay Miner. 15, 179.
Holmboe, M., Wold, S., Jonsson, M., 2012. Porosity investigation of compacted bentonite using XRD profile modeling. J. Contam. Hydrol. 128, 19–32.
Ichikawa, Y., Kawamura, K., Theramast, N., Kitayama, K., 2004. Secondary and tertial consolidation of bentonite clay: consolidation test, molecular dynamics simulation and multiscale homogenization analysis. Mech. Mater. 36, 487–513.
Imbert, C., Villar, M.V., 2006. Hydro-mechanical response of a bentonite pellets/powder mixture upon infiltration. Appl. Clay Sci. 32, 197–209.
Jellander, R., Marčelja, S., Quirk, J.P., 1988. Attractive double-layer interactions between calcium clay particles. J. Colloid Interface Sci. 126, 194–211.
Karnland, O., Olsson, S., Nilsson, U., 2006. Mineralogy and Sealing Properties of Various Bentonites and Smectite-Rich Clay Materials, Sweden.
Kelch, S.E., Ferrage, E., Lanson, B., Charlet, L., Aristilde, L., 2019. Water trapping dynamics in carbohydrate-populated smectite interlayer nanopores. J. Phys. Chem. C 123, 28816–28827.
Kelch, S.E., Youngman, R.E., Ferrage, E., Basinski, J.J., Wang, J., Aristilde, L., 2021. Quantitative SPECTROSCOPIC ANALYSIS OF WATER POPULATIONS IN THE HYDRATED NANOPORE ENVIRONMENTS OF A NATURAL MONTMORILLonite. J. Phys. Chem. C 125, 26552–26565.
Komine, H., Ogata, N., 2003. New equations for swelling characteristics of bentonite-based buffer materials. Can. Geotech. J. 40, 460–475.
Kozaki, T., Saito, N., Fujishima, A., Sato, S., Ohashi, H., 1998. Activation energy for diffusion of chloride ions in compacted sodium montmorillonite. J. Contam. Hydrol. 35, 67–75.
Kozaki, T., Sato, Y., Nakajima, M., Kato, H., Sato, S., Ohashi, H., 1999. Effect of particle size on the diffusion behavior of some radionuclides in compacted bentonite. J. Nucl. Mater. 270, 265–272.
Kozaki, T., Sawaguchi, T., Fujishima, A., Sato, S., 2010. Effect of exchangeable cations on apparent diffusion of Ca2+ ions in Na- and Ca-montmorillonite mixtures. Phys. Chem. Earth, Parts A/B/C 35, 254–258.
Lagaly, C., 1993. From Clay Mineral cristals to colloidal clay mineral dispersions. Surf. Sci. Series, Coagulat. Flocculat. 47, 427–494.
Laird, D.A., 1996. Model for Crystalline Swelling of 2:1 Phyllosilicates. Clay Clay Miner. 44, 553–559.
Laird, D.A., 2006. Influence of layer charge on swelling of smectites. Appl. Clay Sci. 34, 74–87.
Laird, D.A., Shang, C., Thompson, M.L., 1995. Hysteresis in Crystalline Swelling of Smectites. J. Colloid Interface Sci. 171, 240–245.
Likos, W.J., Wayllace, A., 2010. Porosity evolution of free and confined bentonites during interlayer hydration. Clay Clay Miner. 58, 399–414.
Liu, L., 2013. Prediction of swelling pressures of different types of bentonite in dilute solutions. Colloids Surf. A Physicochem. Eng. Asp. 434, 303–318.
Lubetkin, S.D., Middleton, S.R., Ottewill, R.H., Barnes, P.J., Nadeau, P., Fripiat, J., Fowden, L., Barrer, R.M., Tinker, P.B., 1984. Some properties of clay-water dispersions. Philosophical transactions of the Royal Society of London. Series A, Math. Phys. Sci. 311, 353–368.
Luckham, P.F., Rossi, S., 1999. The colloidal and rheological properties of bentonite suspensions. Adv. Colloid Interf. Sci. 82, 43–92.
Madsen, F.T., 1998. Clay mineralogical investigations related to nuclear waste disposal. Clay Miner. 33, 109–129.
Massat, L., Cuisinier, O., Bihannic, I., Claret, F., Pelletier, M., Masrouri, F., Gaboreau, S., 2016. Swelling pressure development and inter-aggregate porosity evolution upon hydration of a compacted swelling clay. Appl. Clay Sci. 124, 197–210.
Meleshyn, A., Bunnenberg, C., 2005. The gap between crystalline and osmotic swelling of Na-montmorillonite: a Monte Carlo study. J. Chem. Phys. 122, 034705.
Michot, L.J., Bihannic, I., Porsch, K., Maddi, S., Baravian, C., Mougel, J., Levitz, P., 2004. Phase diagrams of wyoming Na-montmorillonite clay. Influence Part. Anisotropy. Langmuir 20, 10829–10837.
Mooney, R.W., Keenan, A.G., Wood, L.A., 1952. Adsorption of water vapor by montmorillonite. II. Effect of exchangeable ions and lattice swelling as measured by X-Ray diffraction. J. Am. Chem. Soc. 74, 1371–1374.

Muurinen, A., 2009. Studies on the chemical conditions and microstructure in reference bentonites of alternative buffer materials project (ABM) in Äspö. In: Report, P.W. (Ed.), Posiva Working Report. Posiva, Äspö, p. 46.
Muurinen, A., Karnland, O., Lehikoinen, J., 2004. Ion concentration caused by an external solution into the porewater of compacted bentonite. Phys. Chem. Earth, Parts A/B/C 29, 119–127.
Norrish, K., 1954. Crystalline swelling of montmorillonite: manner of swelling of montmorillonite. Nature 173, 256–257.
Pusch, R., 1982. Mineral–water interactions and their influence on the physical behavior of highly compacted Na bentonite. Can. Geotech. J. 19, 381–387.
Pusch, R., Karnland, O., Hoekmark, H., 1990. GMM - a General Microstructural Model for Qualitative and Quantitative Studies of Smectite Clays, Sweden, p. 95.
Saiyouri, N., Tessier, D., Hicher, P.Y., 2018. Experimental study of swelling in unsaturated compacted clays. Clay Miner. 39, 469–479.
Sakharov, B.A., Naumov, A.S., Drits, V.A., 1982. X-ray diffraction by mixed-layer structures with a random distribution of stacking faults. Sov. Phys. Dokl. 27, 523.
Sato, H., 2008. Thermodynamic model on swelling of bentonite buffer and backfill materials. Phys. Chem. Earth, Parts A/B/C 33, S538–S543.
Sato, T., Watanabe, T., Otsuka, R., 1992. Effects of layer charge, charge location, and energy change on expansion properties of dioctahedral smectites. Clay Clay Miner. 40, 103–113.
Sauzeat, E., Guillaume, D., Villieras, F., Dubessy, J., Francois, M., Pfeiffert, C., Pelletier, M., Ruck, R., Barrès, O., Yvon, J., Cathelinceau, M., 2001. Caractérisation minéralogique, cristallochimique et texturale de l'argile MX-80. CREGU 95.
Schanz, T., Tripathy, S., 2009. Swelling pressure of a divalent-rich bentonite: Diffuse double-layer theory revisited. Water Resour. Res. 45.
Segad, M., Jönsson, B., Cabane, B., 2012. Tactoid Formation in Montmorillonite. J. Phys. Chem. C 116, 25425–25433.
Shannon, R.D., Prewitt, C.T., 1969. Effective ionic radii in oxides and fluorides. Acta Cryst B25,, 925–946.
Sposito, G., Prost, R., 1982. Structure of water adsorbed on smectites. Chem. Rev. 82, 553–573.
Sposito, G., Skipper, N.T., Sutton, R., Park, S.H., Soper, A.K., Greathouse, J.A., 1999. Surface geochemistry of the clay minerals. Proc. Natl. Acad. Sci. U. S. A. 96, 3358–3364.
Stern, O., 1924. Zur Theorie Der Elektrolytischen Doppelschicht. Z. Elektrochem. Angew. Phys. Chem. 30, 508–516.
Takahashi, Y., Kawamura, K., Sato, T., Kobayashi, I., Ichikawa, Y., 2015. In situ X-ray diffraction observation of smectite hydration under constant volume. J. Nucl. Sci. Technol. 52, 1470–1479.
Tamura, K., Yamada, H., Nakazawa, H., 2000. Stepwise hydration of high-quality synthetic smectite with various cations. Clay Clay Miner. 48, 400–404.
Torikai, Y., Sato, S., Ohashi, H., 1996. Thermodynamic Properties of Water in Compacted Sodium Montmorillonite. Nucl. Technol. 115, 73–80.
Viani, B.E., Low, P.F., Roth, C.B., 1983. Direct measurement of the relation between interlayer force and interlayer distance in the swelling of montmorillonite. J. Colloid Interface Sci. 96, 229–244.
Villar, M.V., 2007. Water retention of two natural compacted bentonites. Clay Clay Miner. 55, 311–322.
Villar, M.V., Lloret, A., 2004. Influence of temperature on the hydro-mechanical behaviour of a compacted bentonite. Appl. Clay Sci. 26, 337–350.
Villar, M.V., Gomez-Espina, R., Gutierrez-Nebot, L., 2012. Basal spacings of smectite in compacted bentonite. Appl. Clay Sci. 65-66, 95–105.
Wang, Z., Liu, L., Neretnieks, I., 2011. A novel method to describe the interaction pressure between charged plates with application of the weighted correlation approach. J. Chem. Phys. 135.
Wang, H., Komine, H., Gotoh, T., 2022. A swelling pressure cell for X-ray diffraction test. Géotechnique 72, 675–686.
Warr, L., Berger, J., 2007. Hydration of bentonite in natural waters: Application of "confined volume" wet-cell X-ray diffractometry. Phys. Chem. Earth, Parts A/B/C 32, 247–258.
Watanabe, T., Sato, T., 1988. Expansion characteristics of montmorillonite and saponite under various relative humidity conditions. Clay Sci. 7, 129–138.
Wilson, J., Cuadros, J., Cressey, G., 2004. An in situ time-resolved XRD-PSD investigation into Na-montmorillonite interlayer and particle rearrangement during dehydration. Clay Clay Miner. 52, 180–191.
Yamada, H., Nakazawa, H., Hashizume, H., Shimomura, S., Watanabe, T., 1994. Hydration behavior of Na-smectite crystals synthesized at high pressure and high temperature. Clay Clay Miner. 42, 77–80.
Zhang, Z.Z., Low, P.F., 1989. Relation between the heat of immersion and the initial water content of Li-, Na-, and K-montmorillonite. J. Colloid Interface Sci. 133, 461–472.
Zhang, C., Lu, N., 2018. What is the range of soil water density? Critical reviews with a unified model. Rev. Geophys. 56, 532–562.